2. 1. 3 MEBT1, DTL, SDTL

2. 1. 3. 1 MEBT1

A medium-energy beam-transport line (MEBT) between the RFQ and the DTL was designed [1, 2]. It was modified as MEBT1 according to the change in the peak current. It has three essential tasks: the first is to match the beam from the RFQ to the DTL acceptance in 6-D phase spaces; the second is to chop the macropulse for beam injection into the ring; the third is to measure the beam qualitatively. Figure 2.1.3.1.1 shows the required pulse structure for the linac beam. It is comprised of two kinds of pulse trains: a short pulse of 455 nsec made by a chopping system in the MEBT and a long pulse of 500 μsec delivered from the RFQ. Thus, how to make a chopped short beam pulse is one of the main issues in the design. Here, the modified design is presented on the assumption of both the utilization of an rf chopper [3] and a future upgrade scheme with an anti-chopper [4].

2. 1. 3. 1. 1 Beam-line design

A modified TRACE 3-D [5] was utilized in the beam line design, in which a new element (rf deflector) was incorporated for describing the beam deflection behavior. MAFIA [6] was used to design the deflector cavity (RFD) and to provide field distribution data for TRACE 3-D. The amplitude distribution of the deflecting electromagnetic field along the beam line is read into TRACE 3-D for field generation. In this way, the fringe fields (E and B) of the electrode can be taken into account, which partially compensate for the deflecting efficiency. In the MEBT design, unchopped beam quality conservation and a high deflection efficiency for RF deflector were always pursued.

Figure 2.1.3.1.2 shows a layout of the MEBT1. The results of a TRACE 3-D calculation are shown in Fig. 2.1.3.1.3. Detailed parameters are listed in Table 2.1.3.1.1. In Fig. 2.1.3.1.3, a beam scraper for the chopped beam will be positioned just before the fifth Q-magnet (Q-5).

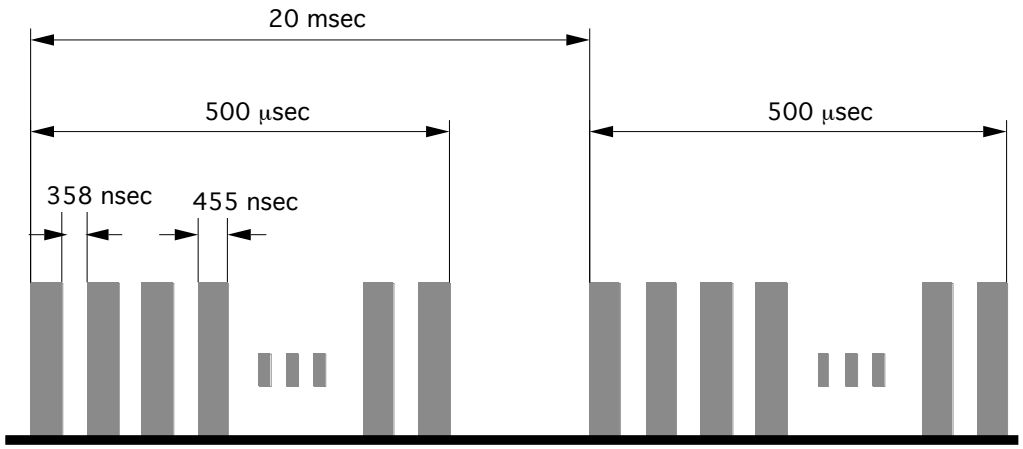

Fig. 2.1.3.1.1 Required time structure of the linac beam pulse. A pulse length is 500 μsec. A repetition rate is 50 Hz. A chopping ratio of 56% and a ring rf frequency of 1.23 MHz are assumed.

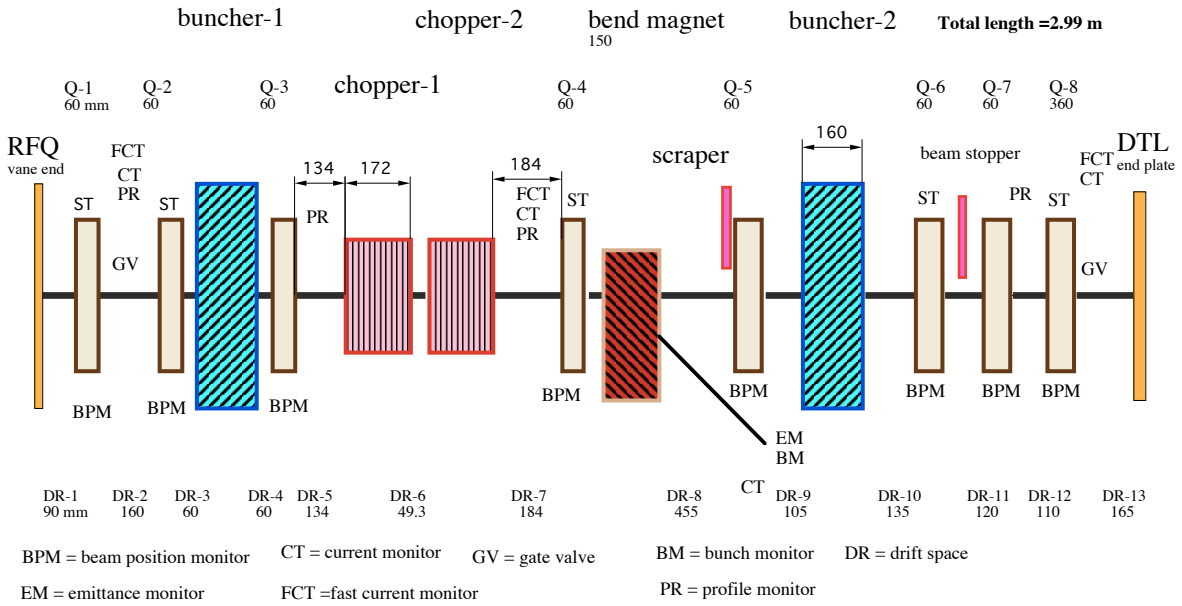

Fig. 2.1.3.1.2 Layout of the MEBT1.

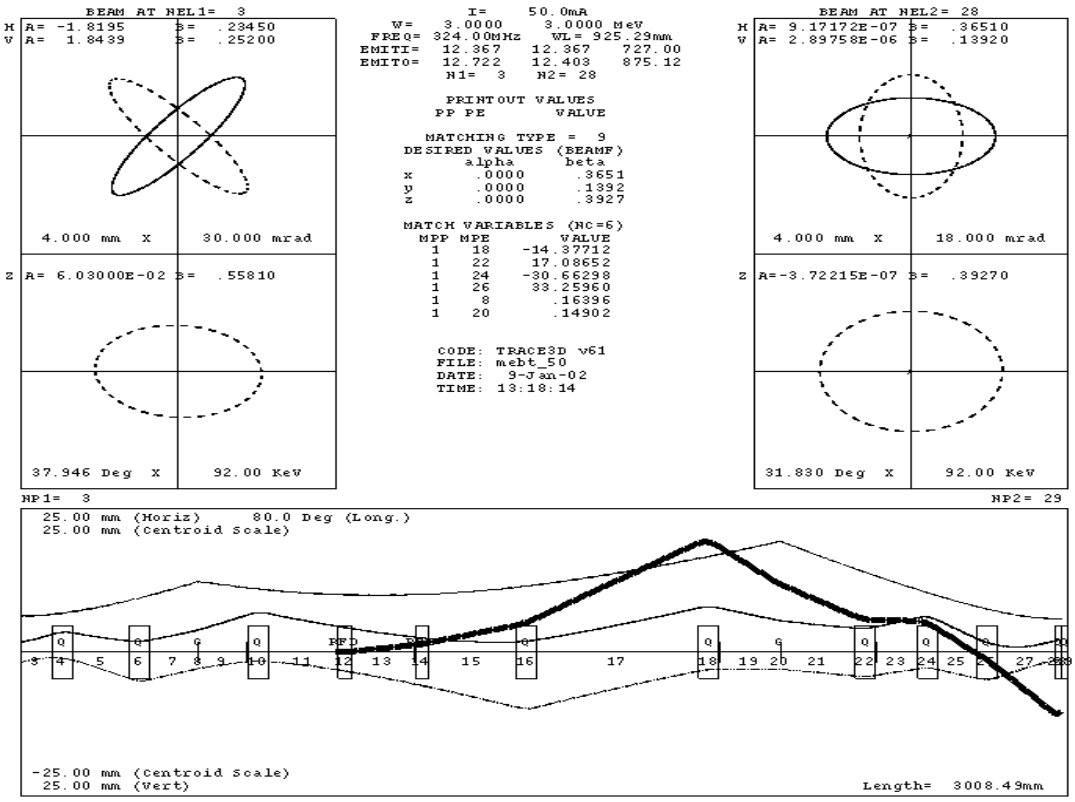

Fig. 2.1.3.1.3 TRACE 3-D output of MEBT1. The upper left gives the input beam phase spaces and the upper right shows the matched beam with the acceptance of DTL. The bottom shows the beam profiles in the z-, x- and y-directions, respectively. The coarse line traces the beam centroid deflected by two rf choppers.

The first half of the beam line, upstream of the scraper, is mainly tuned for achieving a large separation between a chopped beam and an unchopped one at the scraper. Except for the head and tail part of the bunch, the edge separation between a full-chopped beam and an unchopped one is 4 mm at the scraper, when both RFDs have a deflecting field of 1.6 MV/m (corresponding to 22 kW input power). The deflection is initiated by the two RF deflectors with an angle of 5.3 mrad for each, and is then amplified three times by the quadrupole. Downstream of the quadrupole, the deflection angle becomes 33.1 mrad. The first three Q magnets can be adjusted for obtaining a small beam profile in the x-direction at the fourth Q magnet, aimed at a slight defocusing for the beam envelope but larger defocusing for the beam centroid. They should also be sure that the beam envelope dose not become too large in the y-direction. The final four Q magnets can be adjusted for transverse beam matching to the DTL acceptance. Two bunchers can achieve matching in the longitudinal phase space.

Table 2.1.3.1.1 Parameters of the MEBT1 for three kinds of peak currents.

	Gradient/Voltage (T/m) (MV/m) (MV)			Length(mm)
	0mA	10mA	50mA	
Drift 1				90
Q 1	37(F)	35	38	60
Drift 2				160
Q 2	27(D)	30	32	60
Drift 3				60
Buncher 1	0.078	0.125	0.164	160
Drift 4				60
Q 3	17.5(F)	18	20	60
Drift 5				134
RFD 1	1.6(in x)	1.6	1.6	172
Drift 6				49.3
RFD 2	1.6(in x)	1.6	1.6	172
Drift 7				184
Q 4	11.5(D)	12	13	60
Drift 8				465
Q 5	10.8(F)	12.2	14.4	60
Drift 9				105
Buncher 2	0.080	0.127	0.150	160
Drift 10				135
Q 6	20.2(D)	16.9	17.1	60
Drift 11				120
Q 7	30.25(F)	29.3	30.7	60
Drift 12				110
Q 8	27.12(D)	31	33.3	60
Dirft 13				165

Some misalignments both between the RFQ and the MEBT1 and among the elements in the MEBT1 are inevitable. Thus, five steering magnets were installed.

In the MEBT1, sufficient space is required for beam diagnostics and mechanical connections of the transport elements. It is necessary to measure the beam properties during long-term operation. To do this, the sixth drift space is sufficiently long for the insertion of a bending magnet, which leads the beam to a diagnostics beam line.

2. 1. 3. 1. 2 Chopper Design

The RF defelector (RFD)[3] is chosen as a chopper for the following reasons:

1. It is very compact and can provide a high deflecting field.
2. The achievable rising time is about 15 nsec. Although it is not very fast, the necessity of a very fast rising time will disappear with the advanced design using an anti-chopper system.
3. Very stable operation can be expected, since the reliability of the solid-state rf power amplifier is extremely high.
4. Many requirements for the chopped-pulse operation mode can be easily satisfied, since it can be achieved by controlling a low-level rf switch operation.

The detailed design is reported in ref. [5]. The required rf power (P) is inversely proportional to R_s/Q_0, as

$$P = \frac{V^2}{\omega_0 \tau \left(R_s / Q_0 \right)}$$

where R_s is the transverse shunt impedance and Q_0 the unloaded quality factor, τ the rising time and V the deflecting voltage. Therefore, the optimum geometry should have R_s/Q_0 as large as possible for low power and short rising time. A cavity geometry has been found with R_s= 4.7 MΩ and Q_0= 10,650. To obtain a rising time of less than 10 ns, the cavity should have a loaded Q_L of about 10. To realize such a low loaded Q value, two large input/output loops are adopted, which are placed asymmetrically with respect to the middle plane. The cavity geometry is shown in Fig. 3.1.2.3.3 of section 3.1.2.3. For an input power of 22 kW, a HFSS simulation gave a deflection field of 1.6 MV/m in the deflecting gap, which is required for sufficient beam separation between a normal beam and a chopped one. Taking account of a phase length of about 27°, the required rf power becomes higher. If the head and tail of the bunch must meet a full deflecting field of 1.6 MV/m, the required power is 27 kW. In the case that a slightly higher loaded Q is allowed in an anti-chopper scheme, the required power becomes lower. For instance, the required input power is 18 kW if the loaded Q is 15.

2. 1. 3. 1. 3 Analysis on unstable particles

A part of the deflected bunches during the transient time of the RFD may not be stopped by the scraper due to insufficient deflection. Since these particles, named unstable particles, will be injected into the peripheral part of the DTL transverse acceptance, they may be accelerated up to a high energy, and become either lost or get into the ring. Thus, it is very crucial for the chopper to have as few as possible unstable particles during the rf rising and falling times. There are three methods to reduce the number of unstable particles injected into the ring:

1. achieve a fast rising time, resulting in a decrease in the number of bunch during the transient times,
2. utilize a larger rf exciting power in order to obtain the design field level within a shorter rising time, and
3. scrape any unstable particles by using additional scrapers located among the rf structures.

A detailed study concerning the behavior of unstable particles is reported in ref. 1. The main results are as follows:

1. all deflected particles are stopped by the scraper in the MEBT when the deflecting field is higher than 80% of the design value,
2. almost all particles are injected into the DTL acceptance when the deflecting field is less than 30% of the design value,
3. a part of the bunch is injected into the DTL acceptance when the deflecting field is from 30 to 80% of the design value, and
4. if some additional scrapers are utilized among rf structures less than 70 MeV, the number of unstable particles decreases by about ten times.

It should be pointed out that the problem of unstable particles can be solved if we adopt an upgrade scheme with the anti-chopper described in section 2.1.3.1.6.

2. 1. 3. 1. 4 Buncher design

In the MEBT1 design, two bunchers should provide effective bunch voltages of E_0TL=0.164 and 0.150 MV for the first and second bunchers, respectively. Two single cavities of the same geometry are used for simplicity. According to the beam envelope at the first buncher, a relatively large bore-radius of 15 mm is chosen. The cavity length is 160 mm in the beam passing direction in order to obtain a large shunt impedance. Low Kilpatrick multiplication is desired in order to avoid any possible breakdown. Thus, the gap length between the noses is 18 mm. SUPERFISH results show that the cavity can generate an effective voltage for the first buncher with an input power of 6.7 kW. The maximum surface electric field is just equal to the Kilpatrick limit at 324 MHz.

2. 1. 3. 1. 5 Analyzer line design

A bending magnet is installed between the RFD and the scraper. The analyzing system consists of a bending magnet of 45 degrees, a transverse emittance monitor using double slits and a bunch-length monitor. The main purposes of the line are as follows:

1. distinguish and analyze the RFQ beam,
2. measure the average energy,
3. measure the energy spread,
4. measure the transverse emittances,
5. measure the bunch length, and
6. measure the longitudinal emittance.

A detailed method for measurements using both the buncher voltage as a free parameter and a three-dimensional beam-simulation code including a bending magnet was proposed.

2. 1. 3. 1. 6 Upgrade with an anti-chopper

The adoption of an anti-chopper is a good choice for solving the problem of the unstable particles. Theoretically, an anti-chopper system can cancel all unstable particles produced during the transient times.

A MEBT1 with an anti-chopper was designed. It accomplishes matching and chopping, as well as canceling any unstable particles. To maintain the beam quality, the additional increase in the length of the transport line is not too much. This is a benefit of the asymmetric design. The feasibility of the asymmetric scheme was proved [4]. There are two specific features in the anti-chopper design:

1. the cancellation of unstable particles, and
2. a decrease in the importance of a very fast rise time, which, in turn, allows less rf power because of a higher loaded Q-value of the RFD.

Figure 2.1.3.1.4 shows the design of MEBT1 with an anti-chopper. The total length is about 3.8 m. The first half of the beam line, upstream of Q-5, is mainly aimed at a large separation between the chopped beam and the unchopped one at the scraper. The configuration of the elements in this part is the same as for the design without an anti-chopper. The second part of the beam line, downstream of Q-5, should accomplish two tasks: returning the partly deflected beam back to beam axis and matching the unchopped beam to the acceptance of the DTL.

The RFD cavity was adopted as an anti-chopper. The electrode gap of the anti-chopper increased to 12mm, while that of the chopper is 10 mm. A larger gap is required for suppressing beam losses on the electrode. In the design in Fig. 2.1.3.1.4, a deflecting field of 1.7 MV/m is adopted in both anti-choppers. To produce this field, the required rf power is about 27 kW if the loaded Q-value is about 10. It was shown that the beam-line parameters from the fifth quadrupole magnet (Q-5) to the anti-chopper can be tuned for compensating the additional deflection when the input power of chopper is changed, instead of changing the input power of the anti-chopper [4]. In this case, matching with the acceptance of the DTL

can be achieved by the last four quadrupole magnets. In normal operation, it is more convenient to change the input power of the anti-chopper in connection with that of the chopper.

There are three bunchers in the beam line to keep the bunch length as short as possble. Two bunchers are needed for matching the longitudinal phase space to the acceptance of DTL. Three bunchers make it easy to control the bunch length at the deflector, and also to make the bunch length close to each other at the choppers and anti-choppers.

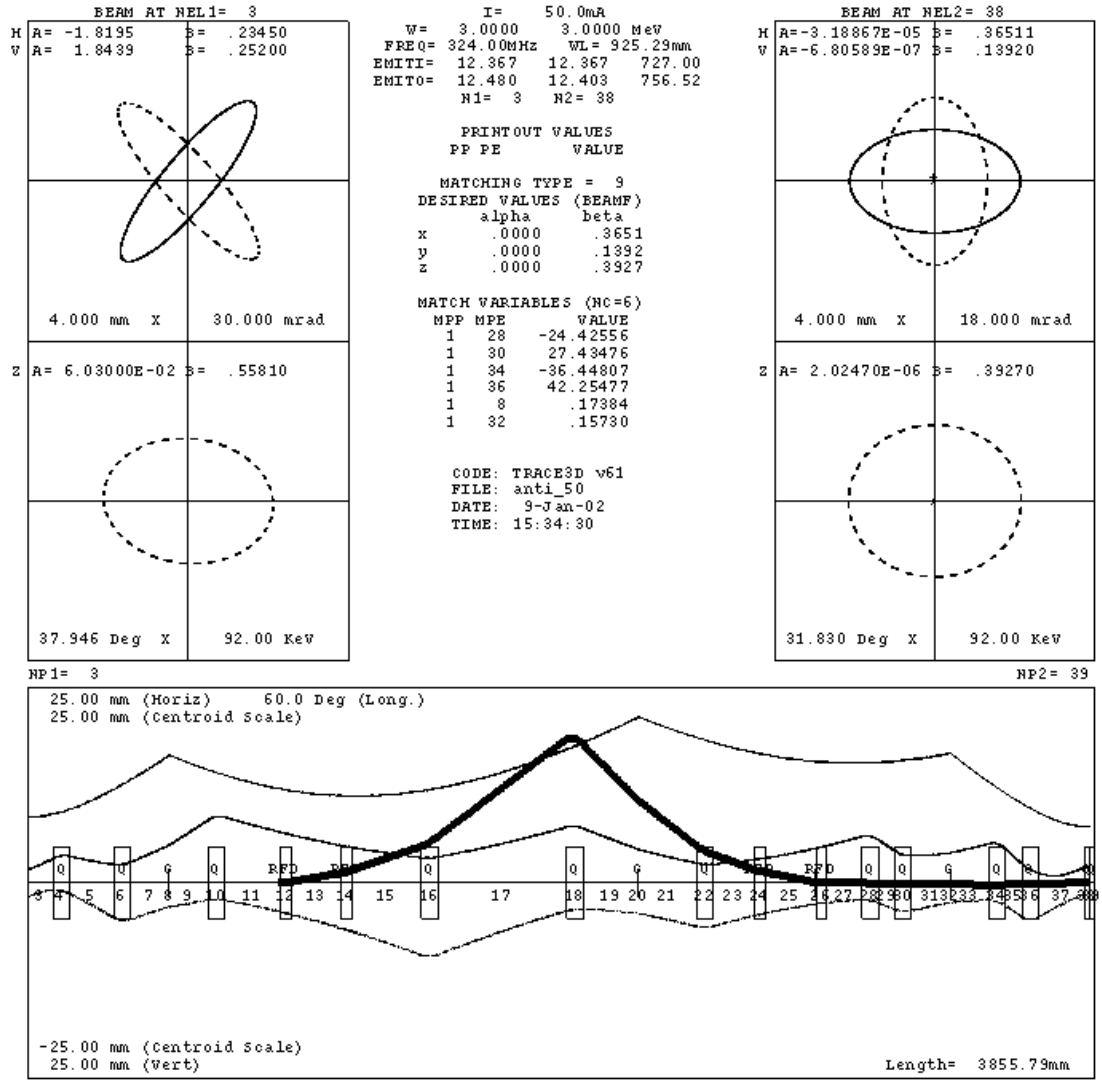

Fig. 2.1.3.1.4 TRACE 3-D output of the MEBT1 with anti-choppers. The upper left gives the input beam phase spaces and the upper right shows the matched beam with the acceptance of the DTL. The bottom shows the beam profiles in the z-, x- and y-directions, respectively. The coarse line traces the beam centroid deflected by two rf choppers and two rf anti-choppers.

2. 1. 3. 1. 7 Beam dynamics simulation

The beam dynamics of the beam line has been studied using PARMILA[7]. Figure 2.1.3.1.5 shows the simulation results of the emittance growth along the MEBT1. Although anti-choppers have been added and the total length increased to 3.8 m, the rms emittance growth is still less than 16%. Figure 2.1.3.1.6 shows the phase space of a 60% deflected beam at the entrance of the DTL. It can be seen that the partly deflected beam is returned back to the beam axis by the anti-chopper.

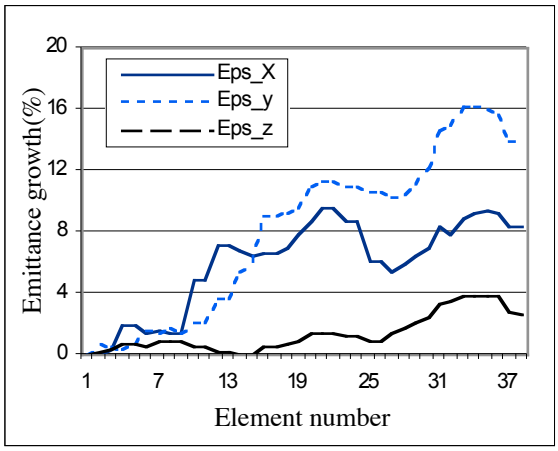

Fig. 2.1.3.1.5 Rms emittance growth along the MEBT1 beam line.

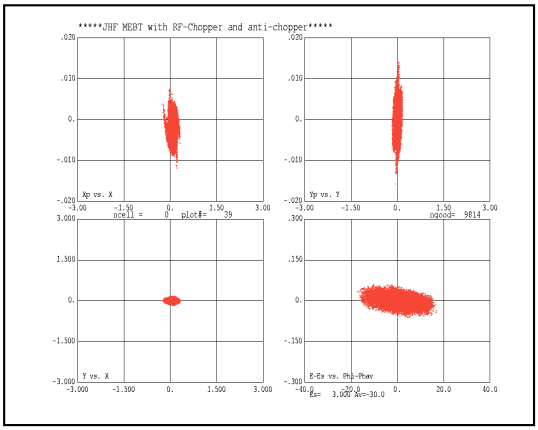

Fig. 2.1.3.1.6 Phase space of a beam deflected by the chopper and anti-chopper at the entrance of the DTL.

References

[1] JHF Project Office, "JHF Accelerator Design Study Report", KEK Report 97-16 (JHF-97-10), 1998.

[2] S. Fu and T. Kato, "Design study on a medium-energy beam-transport line for the JHF proton linac," NIM **A 457** (2001)423.

[3] T. Kato, New Design of an RF Beam Chopper, Proc. of 7th Symp. on Acc. Sci. & Tech. (1989)288.

[4] S. Wang, S. Fu and T. Kato,"Design of a Medium-Energy Beam-Transport Line with an Anti-Chopper for the JAERI/KEK Project," Proc. 26th Linear Accelerator Meeting in Japan, p.79 (2001).

[5] S. Fu and T. Kato, "RF-chopper for the JHF proton linac," **NIM A** (2000)296.

[6] T. Weiland, Part. Accel. , Vol.17 (1995)227.

[7] H. Takeda, LA-UR-98-4478 (1998).

2. 1. 3. 2 DTL and SDTL

2. 1. 3. 2. 1 Introduction

The most important issue of the medium-energy part of the linac (from the exit of the MEBT to the entrance of the ACS) is to realize stable operation without any beam losses, thus satisfying the requirements for beam quality. For realizing the requirements, we have chosen four strategies:

1. an operating frequency higher than that of the conventional DTL,
2. a balanced focusing scheme between the transverse and longitudinal focusing based on the equipartitioning theory, by using both pulsed electromagnets and sufficiently large bore-hole diameters,
3. a high tuning ability by varying the transverse focusing strength of the FD scheme in the DTL and a doublet focusing scheme in the SDTL, and
4. requiring an accelerating field with high stability.

According to these strategies, the main beam-dynamics parameters of the linac were determined.

2. 1. 3. 2. 2 Cell geometry

The cell geometries of the DTL and the SDTL were optimized by using SUPERFISH, while keeping the main shapes constant along the linac, except for the bore radius. It has some merits both in eliminating any small transition effects due to changes in the geometries of the rf structures and in reducing the construction cost. We assume five conditions in optimizing the DTL cell geometry from 3 to 50 MeV:

1. the diameter of the DTL tank remains constant,
2. the diameter of the drift tube remains constant,
3. a flat surface angle for both end faces of the drift tube is used in order to obtain more space for installing focusing magnets and reducing the maximum electric field on the surface,
4. the diameters of the bore hole increase as the energy increases in order to avoid beam loss when the equipartitioning focusing scheme is applied, and
5. the effects of the stem are included in the transit-time factors calculated with SUPERFISH.

Table 2.1.3.2.1 Main parameters of the cell geometry of the DTL and SDTL.

	DTL	SDTL	
Tank diameter	560	520	mm
Drift-tube diameter	148	92	mm
Bore radius	6.5 – 13	18	mm

The geometrical parameters mentioned above are related to the mechanical design of the DTL. Thus, they were finally determined by taking account of the calculated results and the engineering issues. The conditions mentioned above, except for the fourth item, are also applied to the SDTL cell geometry. The main parameters of the cell geometry are listed in Table 2.1.3.2.1.

2. 1. 3. 2. 3 DTL tank parameters

The main DTL tank parameters are listed in Tables 2.1.3.2.2 -3. The accelerating fields in the DTL were determined based on three conditions:

1. the total rf power consumption with a 50-mA beam in a tank is as large as about 2 MW so as to obtain a wide linear feedback operating region for a 2.5-MW klystron, assuming three klystrons for DTL acceleration from 3 to 50 MeV,
2. the equipartitioning condition at the DTL injection point is satisfied under the expected emittances and transverse focusing strength,
3. a smaller accelerating field is desirable from the viewpoint of long-period stable operation in connection with a discharge problem.

Table 2.1.3.2.2 Parameters of the DTL and SDTL.

	DTL	SDTL	
Frequency	324	324	MHz
Injection energy	3	50.1	MeV
Output energy	50.1	190.8	MeV
Accelerating field	2.5 - 2.9	2.53 -3.74	MV/m
Stable phase	30 - 26	27	degree
Number of tank	3	32	
number of cells	146	160	
Total length	27.12	91.17	m
Structure length	26.68	65.69	m
Drift length	0.19 - 0.25	0.60 - 1.02	m
Bore radius	6.5 – 13	17	mm
Rf driving power	3.30(*)	16.6	MW
Beam power (50mA)	2.35	7.04	MW
Total power (50mA)	5.65	23.6	MW
Number of klystron	3	16	
Acceptance			
Ax (normalized 90%)	8.7	21.3	π mm-mrad
Ay (normalized 90%)	8.8	18.6	π mm-mrad
Az (normalized 90%)	9.9	40.4	π MeV-deg
Focusing method	Equipartitioned focusing		
Space between DTL and SDTL	1 βλ = 0.29 m		

2. 1. 3. 2. 4 Focusing design

Both the transverse and longitudinal focusing parameters are determined based on equipartitioning theory combined with coupled envelope equations for the bunched beam, written as (refs. [1-3]):

$$k_{x0}^2 a - \frac{3}{2}\frac{Nr_c}{\beta_0^2\gamma_0^3}\frac{1}{az_m}\left(1-\frac{g_0}{2}\frac{a^2}{\gamma_0^2 z_m^2}\right) - \frac{\varepsilon_{nx}^2}{\beta_0^2\gamma_0^2 a^3} = 0 \quad ,$$

$$k_{z0}^2 z_m - \frac{3}{2}\frac{Nr_c}{\beta_0^2\gamma_0^5}\frac{g_0}{z_m^2} - \frac{\varepsilon_{nz}^2}{\beta_0^2\gamma_0^6 z_m^3} = 0 \quad ,$$

$$r_c = \frac{q^2}{4\pi\varepsilon_0 mc^2} \quad ,$$

$$g_0 = 2\frac{z_m^2}{a^2}M_z \quad .$$

Here, k_{x0} and k_{z0} are the zero-current wave numbers for transverse and longitudinal oscillations, ε_x and ε_z the rms emittances of the transverse and longitudinal phase spaces, *a* and z_m the radii of the bunch in the transverse and longitudinal directions, N the number of particles in a bunch, M_z the ellipsoidal form factor, q the unit charge, ε_0 the absolute permittivity of free space, c the velocity of light, β_0 the relative velocity and γ_0 the relativistic parameter. The wave numbers, including space-charge effects, are written as

Table 2.1.3.2.3 Parameters of the DTL tanks.

DTL Tank number	1	2	3	
Injection energy	3.0	19.716	36.717	MeV
βin	0.0797	0.2017	0.2717	
Output energy	19.716	36.717	50.078	MeV
βout	0.2017	0.2717	0.3141	
Tank length	9.921	9.440	7.323	m
Number of cells	76	43	27	
Number of post couplers	36	42	26	
Rf driving power (*)	1.06	1.17	1.07	MW
Beam power (50mA)	0.84	0.85	0.67	MW
Total power (50mA)	1.90	2.02	1.74	MW
Accelarating field	2.5	2.7	2.9	MV/m
Stable phase	-30	-26	-26	
Drift space	1	1	0	βλ
	0.187	0.251		m

(*)including a factor of 1.3

$$k_x^2 = k_{x0}^2 - \frac{3}{2}\frac{Nr_c}{\beta_0^2\gamma_0^3}\frac{1}{a^2 z_m}\left(1 - \frac{g_0}{2}\frac{a^2}{\gamma_0^2 z_m^2}\right).$$

$$k_z^2 = k_{z0}^2 - \frac{3}{2}\frac{Nr_c}{\beta_0^2\gamma_0^5}\frac{g_0}{z_m^3}.$$

Therefore, the focusing parameters as well as the beam parameters should be calculated cell by cell using the initial parameters given at the entrance of the linac.

Table 2.1.3.2.4 Parameters of the SDTL tanks.

N	Win MeV	betain	Wgain MeV	E_0 MV/m	CL m	TANKL m	drift m	TOTL m	Pw MW	Pb MW	Ptot MW
1	50.08	0.3141	2.71	2.53	0.291	1.471	0.596	1.47	0.174	0.136	0.310
2	52.79	0.3219	2.76	2.53	0.298	1.506	0.610	3.57	0.179	0.138	0.316
3	55.55	0.3295	3.03	2.73	0.306	1.543	0.625	5.73	0.213	0.151	0.365
4	58.57	0.3376	3.08	2.73	0.313	1.580	0.639	7.93	0.219	0.154	0.373
5	61.65	0.3455	3.37	2.95	0.320	1.618	0.655	10.19	0.262	0.169	0.431
6	65.02	0.3540	3.42	2.95	0.328	1.657	0.670	12.50	0.269	0.171	0.441
7	68.45	0.3623	3.75	3.19	0.336	1.696	0.687	14.87	0.324	0.188	0.511
8	72.20	0.3710	3.80	3.19	0.344	1.736	0.703	17.29	0.332	0.190	0.523
9	76.01	0.3796	4.15	3.44	0.352	1.777	0.719	19.77	0.397	0.208	0.605
10	80.16	0.3887	4.20	3.44	0.360	1.818	0.736	22.31	0.408	0.210	0.618
11	84.36	0.3975	4.62	3.74	0.369	1.861	0.753	24.90	0.495	0.231	0.726
12	88.98	0.4069	4.66	3.74	0.377	1.903	0.770	27.56	0.509	0.233	0.742
13	93.65	0.4161	4.71	3.74	0.386	1.945	0.786	30.27	0.522	0.235	0.758
14	98.35	0.4249	4.74	3.74	0.394	1.986	0.802	33.04	0.536	0.237	0.773
15	103.09	0.4336	4.77	3.74	0.402	2.025	0.818	35.87	0.549	0.239	0.788
16	107.87	0.4420	4.80	3.74	0.410	2.064	0.833	38.75	0.562	0.240	0.802
17	112.67	0.4503	4.82	3.74	0.417	2.101	0.848	41.69	0.575	0.241	0.817
18	117.49	0.4583	4.84	3.74	0.425	2.138	0.862	44.67	0.588	0.242	0.830
19	122.34	0.4660	4.86	3.74	0.432	2.173	0.876	47.71	0.601	0.243	0.844
20	127.20	0.4736	4.87	3.74	0.439	2.208	0.890	50.79	0.613	0.244	0.857
21	132.07	0.4810	4.88	3.74	0.446	2.241	0.903	53.93	0.626	0.244	0.870
22	136.96	0.4882	4.89	3.74	0.452	2.274	0.916	57.10	0.638	0.245	0.883
23	141.85	0.4952	4.90	3.74	0.459	2.306	0.929	60.33	0.650	0.245	0.895
24	146.75	0.5020	4.90	3.74	0.465	2.337	0.941	63.59	0.662	0.245	0.907
25	151.65	0.5086	4.90	3.74	0.471	2.368	0.953	66.90	0.673	0.245	0.919
26	156.55	0.5151	4.90	3.74	0.477	2.397	0.965	70.25	0.685	0.245	0.930
27	161.46	0.5214	4.90	3.74	0.483	2.426	0.976	73.64	0.696	0.245	0.941
28	166.36	0.5275	4.90	3.74	0.489	2.454	0.987	77.07	0.707	0.245	0.95
29	171.26	0.5335	4.89	3.74	0.494	2.481	0.998	80.54	0.718	0.245	0.962
30	176.15	0.5393	4.89	3.74	0.499	2.508	1.009	84.05	0.729	0.244	0.973
31	181.03	0.5450	4.88	3.74	0.505	2.534	1.019	87.59	0.739	0.244	0.983
32	185.91	0.5506	4.87	3.74	0.510	2.559	0.000	91.17	0.749	0.243	0.993
	190.779	0.5560							16.601	7.035	23.636

Since it is not easy to vary the accelerating field without any troublesome reactions during operation, the longitudinal focusing strength (k_{z0}) is fixed during operation. For a uniformly distributed field, it varies as the energy increases,

$$k_{z0} \propto \frac{1}{(\beta_0\gamma_0)^{3/2}}.$$

On the contrary, the transverse focusing force varies as

$$k_{x0} \propto \frac{1}{\beta_0}$$

if the zero-current phase advance remains constant along the acceleration. One choice of the variation of the focusing forces is to keep the ratio between the transverse and longitudinal focusing forces constant along the acceleration. In such a case, the transverse focusing force should be decreased along the acceleration in the same manner as the longitudinal force. Then, the transverse beam radius becomes larger than that with the constant phase-advance focusing method. It is also a good choice from the viewpoint of space-charge effects, since the density of the bunch decreases. A demerit of this focusing method is that it requires a larger bore radius. However, from the viewpoint of transitions, the average transverse beam radius varies smoothly from the DTL to the SDTL because of adopting the equipartitioning focusing method in the DTL, although the modulation factor of the envelope becomes larger in the SDTL.

The injection parameters, related to both the beams and structures, are chosen so that the equipartitioning condition is satisfied. The condition is given by

$$\gamma_0 \frac{\varepsilon_{nx}}{\varepsilon_{nz}} \frac{z_m}{a} = 1 \quad \text{or} \quad \frac{k_x \varepsilon_{nx}}{k_z \varepsilon_{nz}} = 1,$$

where the suffix of n means a normalized emittance and k_x and k_z are the wave numbers of the transverse and longitudinal phase oscillations with space-charge. The main focusing parameters along the DTL are plotted in Figs. 2.1.3.2.1 - 2. These parameters are typical. In the operation, the focusing parameters should be calculated again according to the measured injection beam parameters, and carefully adjusted in order to find an optimum quality of the output beam. In such a procedure, the focusing field gradient may be tuned to intermediate values between the results of the equipartitioning focusing method and those of the constant-phase focusing one, as shown in Fig. 2.1.3.2.2, according to the expected values of emittance growths in both phase spaces. A detailed comparison between two focusing schemes is given in ref. 4.

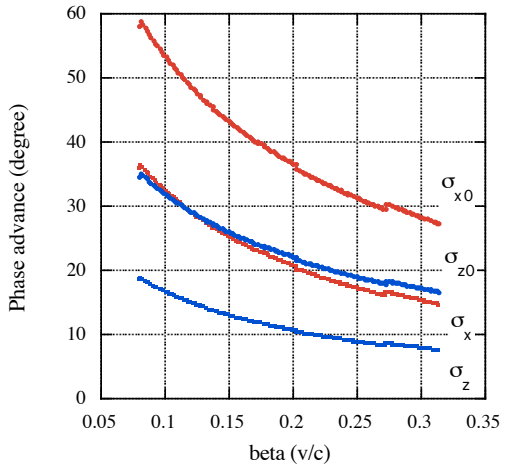

Fig. 2.1.3.2.1 Example of both transverse and longitudinal phase advances for zero and 50 mA beams in the equipartitioning focusing scheme.

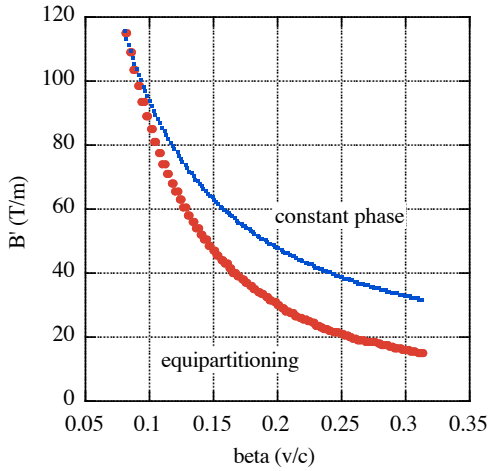

Fig. 2.1.3.2.2 Required magnetic field gradient for both the equipartitioning focusing scheme and the constant-phase advance scheme.

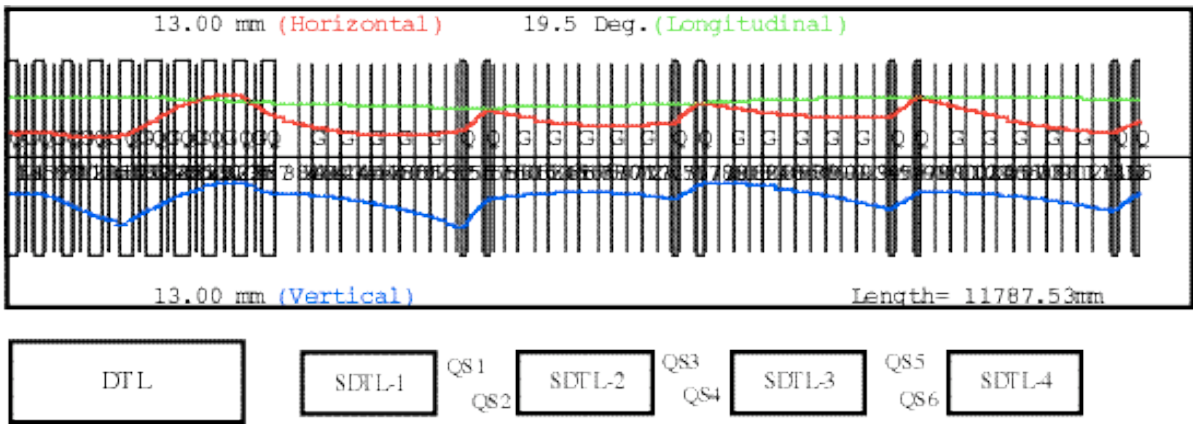

Fig. 2.1.3.2.3 Result of a transverse-matching simulation with the TRACE3D code between the DTL and SDTL. Three curves indicate the beam sizes in three directions: longitudinal (upper), x (middle) and y (bottom).

2. 1. 3. 2. 5 Matching between the DTL and SDTL, and SDTL tank parameters

The SDTL accelerating system consists of a tank of five cells and a two-βλ drift space between two adjacent tanks. The scheme was selected from the viewpoint of both a sufficient transverse focusing force and the available maximum rf power consumption, assuming an equal number of cells for all tanks and the rf excitation of two adjacent tanks by a klystron. Keeping the fundamental configuration throughout the SDTL system is important for avoiding any abrupt changes in the focusing parameters. A doublet focusing system was chosen for SDTL acceleration, since it provides sufficient focusing forces against any strong

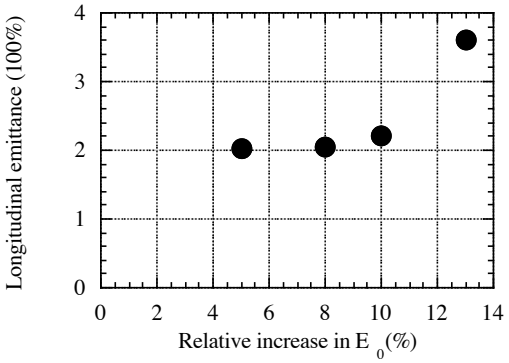

Fig. 2.1.3.2.4 Longitudinal output emittnace of the SDTL as a function of the ratio of the accelerating field increase for every two SDTL-tanks from the entrance.

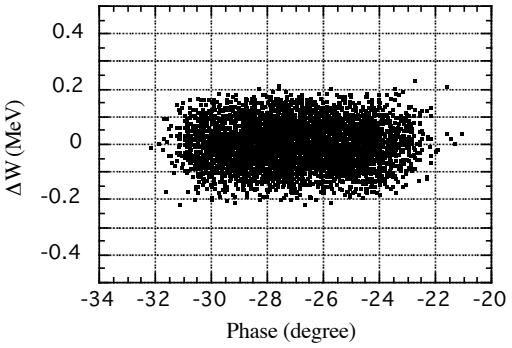

Fig. 2.1.3.2.5 SDTL output emittnace for the nearly matched condition.

space-charge effects. In addition, there is a βλ-drift space between the end of the DTL tank and the entrance of the SDTL. Therefore, some procedures for achieving both transverse and longitudinal matching between the DTL and the SDTL are required. Both matching procedures to be as smooth as possible are desirable from the viewpoint of beam quality in the high-energy region. Transverse matching is achieved by tuning both the last several focusing magnets in the DTL and several sets of the initial focusing magnets among the SDTL tanks (Fig.2.1.3.2.3) The longitudinal matching is achieved by gradually increasing the accelerating field in ten SDTL tanks at the lower energy end. The highest accelerating field was limited by both the maximum available rf power from the klystron and the condition that the surface peak electric field be less than 1.3-times the Kilpatrick limit. The longitudinal emittance increases along the SDTL if the longitudinal matching at the injection part of the SDTL is not sufficiently achieved. Figure 2.1.3.2.4 shows the longitudinal emittance at the exit of the SDTL as a function of the ratio of the accelerating field increase for every two SDTL-tanks from the entrance. Figure 2.1.3.2.5 shows the output emittance in Δϕ–Δw phase space when the field increases by 8% for every two tanks. Figure 2.1.3.2.6 shows the output emittance without a longitudinal matching process.

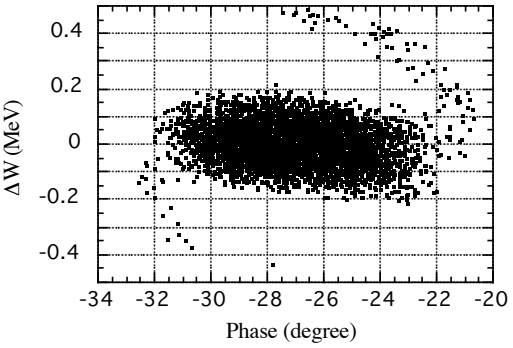

Fig. 2.1.3.2.6 SDTL output emittance without longitudinal matching process.

2. 1. 3. 2. 6 Beam loading of a chopped beam

Some modulation of the accelerating field due to beam loading effects is inevitable in the acceleration of a chopped beam (Fig. 2.1.3.2.7). A sag in the accelerating field ($E_1 - E_2$) by the chopped beam loading can be expressed as

$$\frac{E_1 - E_2}{E_0} = \frac{1}{2}\frac{\omega}{Q_0}\frac{P_b}{P_c}Tf(1-f) = \frac{1}{2}\frac{P_b}{U_0}Tf(1-f),$$

where E_0 is the average accelerating field, ω the rf angular frequency, Q_0 the unloaded Q-value, P_b the beam power, P_c the cavity power, T the chopping period, U the stored energy and f the chopping ratio. The calculated sags are about ±0.1% for both the DTL and the SDTL and ±0.7% for the ACS. The average output energy from the linac will be modulated due to these effects. Since the deviation in the average energy due to the effect in the ACS is about ±70 keV according to a preliminary estimation, the effects are not very obvious.

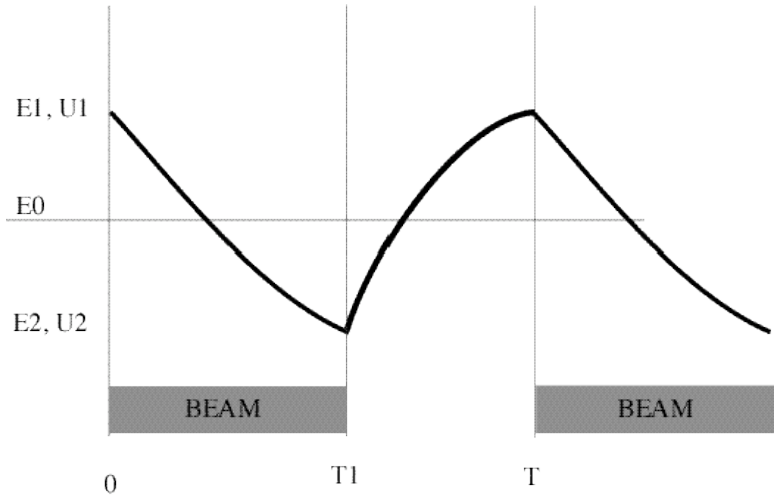

Fig. 2.1.3.2.7 Variation of the accelerating field with chopped beam loading.

2. 1. 3. 2. 7 Beam simulation

Many multi-particle beam simulations for the JHF project have been performed [4, 5]. The advanced LINSAC code [6] was developed for calculating the beam behavior in many types of linacs: DTL, SDTL, ACS and a sc proton linac. The main features of the LINSAC code are as follows:

1. taking account of the space-charge effects by the three-dimensional p-p (particle-to-particle) method,
2. taking account of the field distribution in an accelerating gap calculated with SUPERFISH,
3. time is an independent variable (t-code), and
4. a parallel computer version with MPI can become available.

Both Parmila for the DTL and modified parmila-like codes for both the SDTL and the ACS have also been utilized for studying the beam behavior. Some simulation results are presented in section 2.1.4.3. The initial emittances at the DTL entrance used in the simulation are listed in Table 2.1.2.3.5.

Table 2.1.2.3.5 Normalized rms emittnaces at the DTL injection point.

transverse	longitudinal
0.20 π-mm-mrad	0.15 π -MeV-deg

References

[1] R. A. Jameson, "Beam-Intensity Limitations in Linear Accelerators," IEEE Trans. Nucl. Sci. NS-28, 2408 (1981).

[2] R. A. Jameson, "On Scaling & Optimization of High-intensity Low-beam-loss RF Linacs for Neutron Source Drivers", AIP Conference Proceedings 279 (1993) 969.

[3] M. Reiser, "Theory and Design of Charged Particle Beams," Section 5, John Willy & Sons, 1994.

[4] JHF Project Office, "JHF Accelerator Design Study Report", KEK Report 97-16 Chapter 4 (JHF-97-10), 1998.

[5] T. Kato, "Design of the JHP 200-MeV Proton Linear Accelerator," KEK Report 96-17 (1997).

[6] T. Kato, "Beam Simulation Code Using Accurate Gap Field Distributions in a Drift Tube Linac," Proc. 1994 International Linac Conf., p.523 (1994).